

Shuffle-R1: Efficient RL framework for Multimodal Large Language Models via Data-centric Dynamic Shuffle

Linghao Zhu^{1*}, Yiran Guan^{1*}, Dingkang Liang^{1*}, Jianzhong Ju²,
Zhenbo Luo², Bin Qin², Jian Luan², Yuliang Liu¹, Xiang Bai¹✉

¹Huazhong University of Science and Technology

²MiLM Plus, Xiaomi Inc.

{lh_zhu, yiranguan, dkliang, ylliu, xbai}@hust.edu.cn
{jujianzhong, luozhenbo, qinbin, luanjian}@xiaomi.com

Abstract

Reinforcement learning (RL) has emerged as an effective post-training paradigm for enhancing the reasoning capabilities of multimodal large language model (MLLM). However, current RL pipelines often suffer from training inefficiencies caused by two underexplored issues: Advantage Collapsing, where most advantages in a batch concentrate near zero, and Rollout Silencing, where the proportion of rollouts contributing non-zero gradients diminishes over time. These issues lead to suboptimal gradient updates and hinder long-term learning efficiency. To address these issues, we propose **Shuffle-R1**, a simple yet principled framework that improves RL fine-tuning efficiency by dynamically restructuring trajectory sampling and batch composition. It introduces (1) Pairwise Trajectory Sampling, which selects high-contrast trajectories with large advantages to improve gradient signal quality, and (2) Advantage-based Batch Shuffle, which increases exposure of valuable rollouts through strategic batch reshuffling. Experiments across multiple reasoning benchmarks demonstrate that our framework consistently outperforms strong RL baselines with minimal computational overhead. These results highlight the importance of data-centric adaptations for more efficient RL training in MLLM.

Code — <https://github.com/XenoZLH/Shuffle-R1>

1 Introduction

Inspired by the slow and deliberate thinking process in human cognition, reasoning capabilities empower Large Language Model (LLM) to plan, reflect, and generalize beyond mere memorization (Chu et al. 2025a; Kang et al. 2024). Recent advances have demonstrated that integrating reinforcement learning (RL) into the training of LLMs can significantly enhance such capabilities, particularly in complex domains such as mathematical problem solving and code generation (Guo et al. 2025; Deepmind 2025; OpenAI 2024; Seed et al. 2025). Notably, DeepSeek-R1 (Guo et al. 2025) leverages reward signals derived exclusively from verifiable outcomes to yield impressive performance gains. Beyond textual tasks, RL has also seen increasing application in multimodal domains, including object detection, segmentation,

✉ Corresponding author. *This work was done during the research internship of Linghao Zhu, Yiran Guan, and Dingkang Liang at Xiaomi.

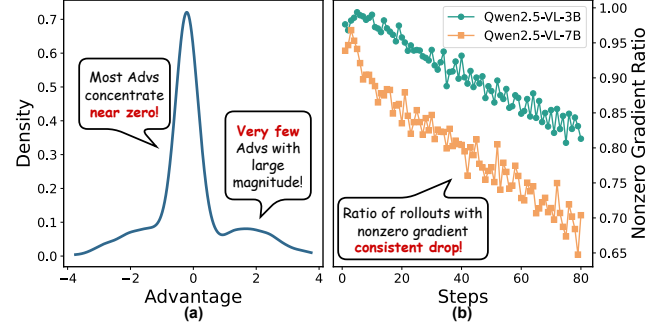


Figure 1: (a): Advantage Collapsing, where most advantages concentrate near zero. (b): Rollout Silencing, where the ratio of rollouts with non-zero gradient consistently drops. The phenomenon gets worse in larger models.

and video understanding (Li et al. 2025; Liu et al. 2025c,b; Wang et al. 2025c), highlighting its potential to support generalizable reasoning across modalities.

Despite the growing interest in RL for LLM and Multimodal LLM (MLLM), several practical challenges remain unresolved, including slow convergence, training instability, and suboptimal efficiency. Recent studies have proposed various improvements, such as empirical optimization of training configurations (Yu et al. 2025), integration of experience replay (Wang et al. 2025a), and refinement of objective functions (Chu et al. 2025b). Other works focus on reward optimization (Liu et al. 2025a; Ma et al. 2025).

However, most of these approaches remain confined to the standard RL training paradigm, where trajectories are uniformly sampled without considering their varying informativeness or difficulty. This static strategy overlooks a crucial insight that not all learning signals are equally valuable, which leads us to consider a fundamental question: *Can dynamically prioritizing trajectories provide richer gradient information and lead to more efficient training?*

Motivated by this question, we examine the current RL training practices and identify two critical yet might underexplored inefficiencies. First, **Advantage Collapsing** emerges when most computed advantages cluster excessively near zero, drowning out informative signals from trajectories with large-magnitude advantages, resulting in weak

or negligible gradient updates (Fig. 1(a)). Second, **Rollout Silencing** arises as the fraction of rollouts contributing non-zero gradients steadily declines during training (Fig. 1(b)), leading to wasted computation and underutilization of data. These two findings demonstrate a pressing need for adaptive mechanisms to prioritize, reuse, and reallocate gradient exposure toward informative samples.

In this paper, we introduce **Shuffle-R1**, an innovative framework designed to dynamically prioritize and amplify critical gradient information. Rather than asking *how to design better rewards*, we try to ask *what data should the model actually update on* during RL fine-tuning. Specifically, Shuffle-R1 introduces two elegantly simple yet highly effective modules: (1) Pairwise Trajectory Sampling, which selects high-contrast trajectory pairs with large-magnitude advantages from an extended rollout pool, concentrating learning signals to mitigate Advantage Collapsing; and (2) Advantage-based Batch Shuffle, which dynamically reshapes training batches to prioritize informative trajectories while down-weighting ineffective ones, alleviating Rollout Silencing to improve data utilization. Our framework is lightweight, modular, and seamlessly integrable with existing RL algorithms. Experiments demonstrate that Shuffle-R1 significantly improves model performance across challenging multimodal reasoning tasks, even surpassing GPT-4o and Claude-3.7 on MathVerse and MathVista. Moreover, it achieves competitive performance to GRPO while requiring only half of the training steps.

In summary, our contributions are three-fold: **1)** We reveal two critical yet underexplored limitations that undermine training efficiency in RL fine-tuning for MLLM, i.e., Advantage Collapsing and Rollout Silencing. **2)** We propose Shuffle-R1, a novel and adaptive RL framework that dynamically selects high-contrast trajectories and reshapes training batches to emphasize informative samples. **3)** Extensive experiments across model scales and both in-domain and out-of-domain benchmarks demonstrate the effectiveness and generalizability of our framework.

2 Related Work

2.1 Large Reasoning Models

Researchers have explored various approaches to equip LLM with reasoning ability. Some early studies performed SFT on complex long chain-of-thought data, leading to performance gains on reasoning tasks (Muennighoff et al. 2025; Ye et al. 2025; Yue et al. 2024; Guo et al. 2024). However, some claim that SFT merely enables the model to memorize the format of reasoning steps and long chains of thought, without fully grasping the ability to reason independently (Chu et al. 2025a; Kang et al. 2024; Ye et al. 2024; Allen-Zhu and Li 2024). Some researchers control the model to generate structured chain-of-thought instead of free generation, achieving systematic step-by-step reasoning output (Xu et al. 2025; Wu et al. 2025; Thawakar et al. 2025). Other works attempted to use test-time scaling like Monte Carlo Tree Search (MCTS) (Yao et al. 2023; Zhang et al. 2024a; Du et al. 2024; Yao et al. 2024) to facilitate complex reasoning by actively extending the output of the model.

Recently, models such as OpenAI o1/o3 (OpenAI 2024), DeepSeek-R1 (Guo et al. 2025), Seed-Thinking (Seed et al. 2025), and Kimi-k1.5 (Team et al. 2025) utilized RL to enable the model to explore independently, stimulating reasoning ability. In particular, DeepSeek-R1-Zero directly conducted RL on pre-trained model without instruction fine-tuning, with verifiable outcome reward functions to replace reward models, achieving surprising reasoning ability. The training algorithms for RL are also constantly being optimized (Yu et al. 2025; Chu et al. 2025b). Our work focuses on a deeper investigation of the efficiency of RL training and puts forward an effective solution to improve both the efficiency and performance of RL training.

2.2 Reinforcement Learning for MLLM

Following the success of DeepSeek-R1, a series of studies have transplanted RL into the training of MLLM and downstream visual tasks, such as Open Vocabulary Object Detection (Liu et al. 2025c), Reasoning Segmentation (Liu et al. 2025b), Video Understanding (Li et al. 2025), Video Localization (Wang et al. 2025c), etc. These works mainly focus on the applicability of RL in downstream tasks. Some other works focusing on improving the general reasoning ability of MLLM have achieved performance improvement on reasoning tasks by collecting a large amount of high-quality data (Meng et al. 2025; Huang et al. 2025; Yang et al. 2025; Zhang et al. 2025; Peng et al. 2025; Tan et al. 2025). These works mainly focus on the organization of high-quality reasoning data and the balance between SFT and RL in the training process.

Some researchers who conduct in-depth research on the RL mechanism have optimized the RL training process from various aspects, including adding contrastive reward mechanism (Li et al. 2025), actively introducing reflection tokens during rollouts (Wang et al. 2025a), optimizing the RL objective function and gradient update mechanism (Chu et al. 2025b), introducing more diverse rollouts (Liu et al. 2025a; Yao et al. 2025), etc. The core objective of these works is to optimize the RL training process. In our work, we propose a novel training framework that introduces dynamic and adaptive selection and resampling to queries and rollouts, reshaping data distribution for better training efficiency and model performance.

3 Preliminaries

Reinforcement Learning in LLM. Reinforcement learning is originally introduced as a post-training technique to align LLM outputs with human preference. Recently, it has been used in fine-tuning stage to improve the reasoning ability of LLMs. Policy gradient algorithm is the most commonly used RL method, whose objective function is to maximize the expectation of return the model gets from the environment. Given a query q , multiple independent sampled responses $O = \{o_1, o_2, \dots, o_N\}$ are sampled from the old policy model $o \sim \pi_{\theta'}(q)$, with rollout size N . Subsequently, the corresponding rewards $R = \{r_1, r_2, \dots, r_N\}$ are obtained for each response, in our case they are calculated by verifiable reward functions. Advantages $\hat{A} =$

$\{A^{\pi_\theta}(r_1), A^{\pi_\theta}(r_2), \dots, A^{\pi_\theta}(r_N)\}$ are calculated to assess the improvement over the current policy model. Importance sampling and clipping are introduced to stabilize the training. The core objective function is defined as:

$$\begin{aligned} \mathcal{J}(\theta) = & \mathbb{E}_{q \sim \mathcal{D}, \{o_i\}_{i=1}^N \sim \pi_{\theta'}(\cdot | q)} \\ & \frac{1}{\sum_{i=1}^N |o_i|} \sum_{i=1}^N \sum_{t=1}^{|o_i|} \left\{ \min [\gamma_t(\theta), \text{clip}(\gamma_t(\theta), 1 - \epsilon, 1 + \epsilon)] \hat{A}_i \right\}, \end{aligned} \quad (1)$$

where

$$\gamma_t(\theta) = \frac{\pi_\theta(o_{i,t}|q, o_{i,<t})}{\pi_{\theta'}(o_{i,t}|q, o_{i,<t})}, \quad (2)$$

$$\hat{A}_i = \frac{r_i - \text{mean}(R)}{\text{std}(R)}, \quad (3)$$

and ϵ is clipping hyperparameter to prevent training collapse.

However, current static RL training paradigm still exhibits limitations. Most of the collected rollouts have advantages sharply concentrated near zero, providing limited signals for gradient update. The proportion of rollouts with non-zero gradient continues to decline throughout the training, introducing invalid updates. These limitations indicate the need for a more efficient training framework.

4 Method

In this section, we begin by further analyzing the existing inefficient issues in training. Then, as illustrated in Fig. 3, we introduce **Shuffle-R1**, which optimizes the training process through two crucial modules: (1) Pairwise Trajectory Sampling and (2) Advantage-based Batch Shuffle.

4.1 Problem Analysis

Advantage Collapsing. Our probe analysis reveals that, contrary to the ideal scenario, most rollouts exhibit advantages sharply concentrated around zero in current RL paradigm, leading to the Advantage Collapsing phenomenon. Such distribution results in weak gradient signals and hampers effective policy updates, as only rollouts with high-magnitude advantages can provide significant gradient signals. Simply increasing the number of rollouts can collect more amount of valuable rollouts and improve performance to some extent (Fig. 2(a)), but also substantially increase the computational overhead without fundamentally resolving the Advantage Collapsing. These findings highlight the need for a dynamic mechanism that can adaptively identify and select valuable rollouts to improve training efficiency.

Rollout Silencing. We observe that the proportion of rollouts contributing non-zero gradients steadily decreases as training progresses, resulting in the Rollout Silencing phenomenon. This is primarily caused by the accumulation of factors such as zero advantages, gradient clipping, and overlong truncation, which further exposes the limitations of static sampling paradigm. By tracking queries of varying difficulty, we find that simple queries tend to converge early, while difficult ones consistently yield low accuracy

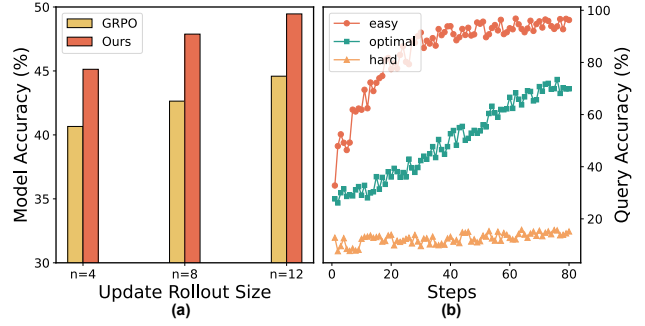


Figure 2: (a) Model accuracy improves with larger rollout sizes. (b) Queries with different difficulties demonstrate varying accuracy during training, their corresponding rollouts have different diversity and qualities consequently.

(Fig. 2(b)). Both cases fail to generate diverse and informative rollouts throughout training, contributing to Rollout Silencing. Moreover, in standard training pipelines, each rollout is used only once for a single gradient update, limiting the model to fully exploit valuable rollouts. Consequently, a dynamic sampling strategy that can adaptively discard ineffective rollouts and queries, while allowing repeated learning from valuable rollouts is of great importance.

4.2 Pairwise Trajectory Sampling

To relieve Advantage Collapsing, we seek to select trajectories that offer stronger learning signals. Since increasing the rollout number enlarges the chance of capturing high-advantage samples, we propose Pairwise Trajectory Sampling (PTS), a data-centric module to selectively amplify valuable learning signals. Rather than evaluating trajectories in isolation, PTS organizes candidate rollouts into structured contrastive pairs. This pairing mechanism captures both high and low advantage signals jointly, forming informative ‘positive-negative’ pairs. Only pairs with the largest advantage contrast are then retained for training. This process ensures that limited update bandwidth is focused on trajectories that are both diverse and gradient-rich.

Given a query q and a rollout size of $2N$, the rollout trajectories group is denoted as $O = \{o_i\}_{i=1}^{2N}$. The corresponding reward and advantage sets are $R = \{r_i\}_{i=1}^{2N}$ and $A = \{\hat{A}_i\}_{i=1}^{2N}$, respectively. To identify informative trajectory pairs, our proposed pairing mechanism follows a simple ‘max-and-min’ principle by matching the trajectory with the highest advantage to that with the lowest, the second highest to the second lowest, and so on. We denote the sorted advantage values in descending order as:

$$A_s = \{\hat{A}_{(i)}\}_{i=1}^{2N}, \quad \text{where } \hat{A}_{(1)} \geq \hat{A}_{(2)} \geq \dots \geq \hat{A}_{(2N)}. \quad (4)$$

Based on this ordering, we construct the pairing set as:

$$P = \{(o_{(i)}, o_{(2N-i+1)})\}_{i=1}^N. \quad (5)$$

In this scheme, the original $2N$ rollouts are easily sorted and reorganized into N pairs. The top-ranked pairs typically consist of trajectories with high-magnitude but opposite-sign advantages, forming contrastive pairs akin to ‘positive-

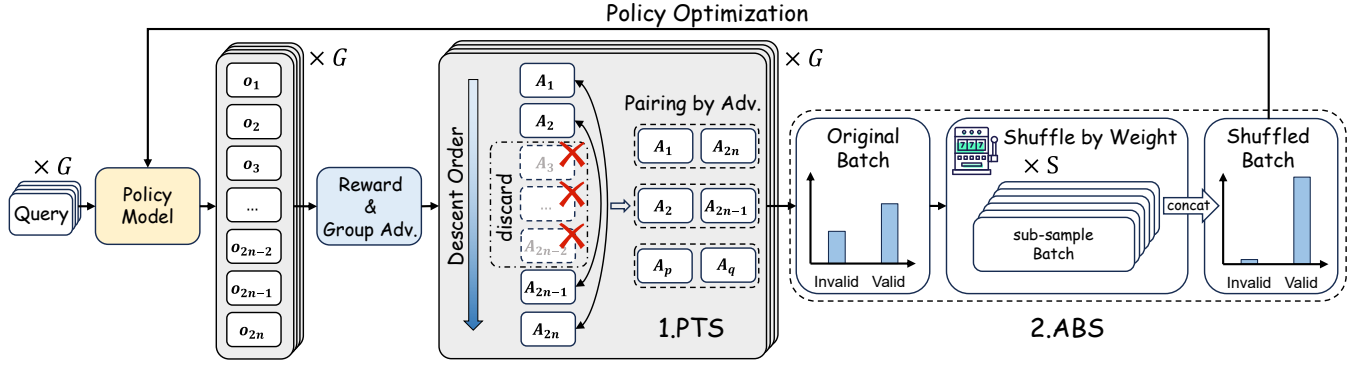


Figure 3: Overview of our proposed Shuffle-R1. After advantage calculation, we first conduct Pairwise Trajectory Sampling to obtain valuable trajectory pairs from original rollout pool, then perform Advantage-based Batch Shuffle to reshape the distribution of valid trajectories in a batch.

negative” samples. In contrast, the bottom-ranked pairs involve trajectories with advantages closer to zero.

As implied by Eq. 1, trajectories with higher absolute advantages contribute more significantly to the gradient update, while those with near-zero advantages have negligible impact. We apply a simple top- k sampling strategy to select a subset of valid pairs:

$$P_v = \{(o_{(i)}, o_{(2N-i+1)})\}_{i=1}^M, \quad M = \alpha N, \alpha \in (0, 1). \quad (6)$$

where α is a hyperparameter controlling the sampling ratio from the pairing set. We only keep the trajectories in the valid set for gradient update.

By introducing a structured contrastive sampling scheme, PTS enables more effective trajectory selection from a broader exploration space without increasing the gradient computation cost. The contrastive pairing not only filters out low-signal trajectories, but also sharpen the model’s policy gradient through direct comparison. PTS shifts the focus of RL fine-tuning from uniform exploration to gradient-informed selection, representing a principled step toward more efficient data usage in RL training.

4.3 Advantage-based Batch Shuffle

While PTS could mitigate Advantage Collapsing and improve RL training performance, the Rollout Silencing issue remains unresolved. To overcome this issue, we propose Advantage-based Batch Shuffle (ABS) module that dynamically reshapes training batches to prioritize and reinforce high-value samples. Rather than relying on static data flow, ABS adaptively redistributes trajectories within each training batch, enabling more frequent updates to trajectories with high learning utility. Built on top of PTS, it serves to magnify the gradient exposure of informative samples, reshaping the training data distribution to achieve better data utilization and training efficiency.

Denote a data batch:

$$B = \{p_i^g = (o_{i,1}^g, \hat{A}_{i,1}^g, o_{i,2}^g, \hat{A}_{i,2}^g, q^g)\}_{i=1 \sim M, g=1 \sim G}, \quad (7)$$

with batch size of $M \times G$. In the standard gradient update process, B is sequentially divided into K mini-batches, each contains MG/K samples.

In our ABS module, we first assign an importance weight to each trajectory pair based on the sum of the absolute advantages:

$$W(p_j) = |\hat{A}_{j,1}| + |\hat{A}_{j,2}|. \quad (8)$$

We then define the sampling probability of each pair $p_j \in P_v$ as:

$$\Phi(p_j) = \frac{W(p_j)}{\sum_{k=1}^{|P_v|} W(p_k)}. \quad (9)$$

Based on the sampling probability, we perform S sub-sampling from original batch B , each sub-sampling has a capacity of T pairs ($2T$ trajectories):

$$B_s = \{p_{s,t}\}_{t=1}^T, \quad \text{s.t. } p_{s,t} \neq p_{s,t'}, \forall t \neq t'. \quad (10)$$

All the sub-sampling batches are sequentially combined to form the *reshuffled* batch $B' = \bigcup_{s=1}^S B_s$. During the ABS process, we set $|B'| = |B|$, i.e., $S \times T = MG$ to ensure the reshuffled batch matches the same size as the original batch. The reshuffled batch will maintain the gradient update paradigm of the original method.

The ABS module optimizes the learning process through Advantage-aware shuffling and Inter-sub-batch resampling. It increases the update frequency of trajectories with higher advantages, maintains diversity while reinforcing high-value samples through repeated exposure. Together, these designs transform each batch into a soft-prioritized structure that better reflects training signal utility.

5 Experiments

5.1 Experimental Setup

Datasets and Benchmarks. We first conduct our experiments on Geometry3K dataset (Lu et al. 2021) (2.1k training samples.) and a subset of MMK12 dataset (Meng et al. 2025) containing the same amount of data, to investigate model performance on limited training resources. Then, we conduct experiments on larger data scale with MM-Eureka dataset (Meng et al. 2025), seeking for better model performance. We randomly select 27k samples from MM-Eureka dataset and mix them with Geometry3K dataset, forming a total of 30k training corpora. All training samples are in free-form format.

Method	Geo3K	Math Avg.	HallBench	ChartQA
Qwen-3B	25.79	41.71	59.83	73.08
+ GRPO	42.64	46.74	63.09	76.20
+ DAPO	45.09	48.08	63.24	76.70
+ Ours	47.88(+22.09)	48.70(+6.99)	63.19(+3.36)	77.04(+3.06)
Qwen-7B	38.12	49.82	65.19	79.84
+ GRPO	52.60	53.13	68.56	80.84
+ DAPO	54.43	54.19	69.29	81.20
+ Ours	55.89(+17.77)	54.63(+4.81)	69.51(+4.32)	81.64(+1.80)

Table 1: Performance of Shuffle-R1 on Geometry3K dataset compared with GRPO and DAPO.

Method	K12	Math Avg.	HallBench	ChartQA
Qwen-3B	42.42	41.71	59.83	73.08
+ GRPO	59.19	48.71	64.14	77.12
+ DAPO	61.42	49.75	65.08	77.00
+ Ours	62.22(+19.80)	50.05(+8.34)	65.72(+5.89)	78.28(+5.20)
Qwen-7B	52.13	49.82	65.19	79.84
+ GRPO	66.15	54.47	67.75	82.48
+ DAPO	68.35	54.52	68.66	82.52
+ Ours	68.78(+16.65)	55.02(+5.20)	69.87(+4.68)	82.60(+2.76)

Table 2: Performance of Shuffle-R1 on K12 dataset compared with GRPO and DAPO.

We first perform evaluation on in-domain test set of Geometry3K and MMK12. Further, as RL is famous for its strong generalizability, we evaluate our model’s performance on the following representative visual reasoning benchmarks: MathVerse (Zhang et al. 2024b), MathVision (Wang et al. 2024), WeMath (Qiao et al. 2024), Math-Vista (Lu et al. 2023), HallusionBench (Guan et al. 2024) and ChartQA (Masry et al. 2022). These benchmarks span across math reasoning, visual perception, and chart understanding. We use MathRuler to evaluate questions with free-form ground truths and Gemini-2.0-Flash-001 (Deepmind 2025) to evaluate questions with multi-choice ground truths.

Implementation Details. We use EasyR1 (Yaowei et al. 2025) as our training codebase. We choose Qwen2.5-VL-3B-Instruct and Qwen2.5-VL-7B-Instruct (Bai et al. 2025) as base model to verify our method’s generalizability on model scales. Parameters of vision encoder are kept frozen. We set update batch size to 128 and rollout batch size (G) to 512. Rollout temperature is set to 1.0 and learning rate is set to $1e - 6$. All experiments are conducted on $8 \times$ H800-80G GPUs. For PTS, we sample 4 trajectory pairs (8 trajectories) from 16 rollouts for each query, striking a balance between training cost and exploration space. For ABS, we set the sub-sampling batch size (T) to 256 pairs (512 query-response trajectories) and the shuffle times (S) to 8. For evaluation, we set the temperature to 0.5 and report the average pass@1 accuracy of 8 tests to reduce randomness.

5.2 Main Results

Comparison with Representative Algorithms. We compare model performance of our method with GRPO (Shao

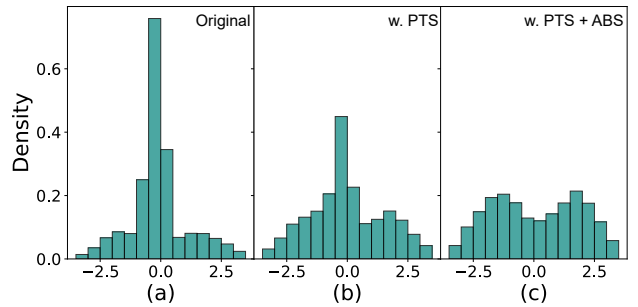


Figure 4: Advantage distribution in a training batch of GRPO and our framework.

et al. 2024) and DAPO (Yu et al. 2025). As shown in Tab. 1, after training on the Geometry3K dataset, the 3B model trained with our method achieved 47.88% accuracy on in-domain test set, with a 5.2% improvement compared to model trained with GRPO and 2.7% improvement compared to DAPO. Similarly, for the 7B model, our method led to 3.3% improvement over GRPO and 1.4% over DAPO, achieving 55.89% accuracy. The superiority of our framework is further highlighted in out-of-domain benchmarks. For out-of-domain math reasoning task, the average accuracy is improved by 1.96% on 3B model and 1.5% on 7B model compared to GRPO, and surpasses DAPO as well. Similar performance gains are also observed on HallusionBench and ChartQA, where the data gap is even further from training data, showing strong generalizability of our framework. Tab. 2 demonstrates similar performance results on K12 dataset, where consistent performance gains are achieved on both in-domain and out-of-domain benchmarks, highlighting our framework’s generalizability on different data distribution.

Comparison with RL-based models. We conduct larger scale experiments on MM-Eureka dataset. As shown in Tab. 3, trained with $30k$ selected data from diverse sources for 150 steps, our 7B model exhibits a substantial accuracy gain over the base model (Qwen2.5-VL-7B). Moreover, it outperforms a series of open-source 7B competitors who also adopt RL training strategies, e.g. MM-Eureka with direct RL and VLAA-Thinker with RL after cold-start SFT. Notably, our model achieves competitive or superior performance on several benchmarks compared to leading close-source models, for instance, Claude-3.7-Sonnet (Anthropic 2025) and GPT-4o (Achiam et al. 2024). Under the same setting, our 3B variant also demonstrates strong performance, even outperforming several 7B models on certain benchmarks. These results highlight the superiority of our proposed approach in boosting the training efficiency in reinforcement learning.

Efficiency Analysis. The improvement in model performance mainly stems from better training efficiency. Fig. 2(a) in previous section shows that, under the same update rollout size, model trained under our framework significantly outperforms GRPO, indicating more effective utilization of training data. Advantage distribution analysis in Fig. 4

Model	MathVerse	MathVision	MathVista	WeMath	HallBench	ChartQA	Avg.
<i>Close-source</i>							
GPT-4o (Achiam et al. 2024)	50.8	30.4	63.8	68.8	55.0	-	-
o1 (OpenAI 2024)	57.0	60.3	73.9	-	-	-	-
Gemini-2.0 pro (Deepmind 2025)	67.3	48.1	71.3	-	49.8	-	-
Claude-3.7-Sonnet (Anthropic 2025)	52.0	41.3	66.8	72.6	55.4	-	-
<i>Open-Source SFT</i>							
InternVL-2.5-8B (Chen et al. 2025b)	39.5	17.0	64.5	-	50.1	79.1	-
InternVL-3-8B (Zhu et al. 2025)	-	29.3	71.6	-	49.9	86.6	-
Qwen2.5-VL-3B* (Bai et al. 2025)	34.8	21.9	58.4	51.7	59.8	73.1	49.9
Qwen2.5-VL-7B* (Bai et al. 2025)	42.6	25.8	67.4	63.5	65.2	79.8	57.4
<i>Cold Start + RL</i>							
R1-VL-7B* (Zhang et al. 2025)	40.1	24.3	62.3	59.8	60.9	76.1	53.9
Vision-R1-7B*† (Huang et al. 2025)	46.1	-	70.8	-	57.8	83.1	-
R1-OneVision-7B* (Yang et al. 2025)	43.0	24.8	61.2	60.6	66.4	77.8	55.2
OpenVLThinker-7B* (Deng et al. 2025)	46.4	24.8	69.7	67.2	59.1	78.4	57.6
VLAA-Thinker-7B* (Chen et al. 2025a)	48.9	26.3	69.9	67.7	67.5	80.1	60.1
<i>Zero RL</i>							
MM-Eureka-Qwen-7B* (Meng et al. 2025)	49.6	27.4	70.6	67.4	66.7	79.0	60.1
MMR1-Math-7B* (Leng et al. 2025)	39.2	31.9	71.5	70.7	69.6	<u>82.0</u>	60.8
ThinkLite-VL-7B* (Wang et al. 2025b)	45.2	28.0	<u>72.4</u>	69.3	<u>70.2</u>	<u>82.0</u>	61.2
VL-Rethinker-7B* (Wang et al. 2025a)	<u>51.7</u>	29.7	72.0	70.1	69.9	79.0	<u>62.1</u>
NoisyRollout-7B-K12* (Liu et al. 2025a)	50.1	28.0	70.9	<u>70.8</u>	70.1	81.4	<u>62.1</u>
Shuffle-R1-Qwen-3B (Ours)	44.2	26.8	70.4	66.5	69.2	79.9	59.5
Shuffle-R1-Qwen-7B (Ours)	53.9	<u>30.0</u>	77.0	72.3	71.0	84.1	64.7

Table 3: Model performance on representative visual reasoning benchmarks. Models marked with “*” are evaluated using our own evaluation scripts with vLLM. †Vision-R1-7B used WeMath and MathVision as training data, its performance on these benchmarks are omitted. Best performance of RL-only models marked with **Bold**, second best with underline.

proves that, PTS effectively mitigates Advantage Collapsing by increasing the proportion of large-magnitude advantages. ABS further optimizes the batch composition, enabling the model to focus on more informative trajectories.

Fig. 5(a) and (b) further probe into training dynamics and demonstrate that our framework consistently achieves higher training and validation accuracy, reaching comparable performance as GRPO but with only half the training steps. Moreover, our framework effectively mitigates the issue of “Rollout Silencing” shown in Fig. 5(c), maintaining a high token utilization rate across all training stages. Fig. 5(d) further illustrates the favorable trade-off between training scale and computational cost of our approach, substantially expanding the RL exploration space with minimal additional overhead.

5.3 Ablation Study

We conduct ablation experiments on Qwen2.5-VL-3B-Instruct using Geometry3K, focusing on two objectives: (1) assessing the contribution of each component in our framework, and (2) validating the impact of key designs.

Effectiveness of Algorithm Design. We assess the effectiveness of proposed PTS and ABS modules by successively introduce them to the baseline. As shown in Tab. 4, in the in-domain Geometry3K test set, PTS demonstrates significant performance gains, improving the model accuracy from 42.64% to 46.21% (+3.57%). When ABS is in-

GRPO	PTS	ABS	Geo3k	Math Avg.	HallBench	ChartQA
✓			25.79	41.71	59.83	73.08
✓	✓		42.64	46.74	63.09	76.20
✓	✓	✓	46.21	47.64	63.40	76.52
			47.88	48.70	63.19	77.04

Table 4: Ablation study on effectiveness of PTS and ABS.

roduced for co-optimization, the model achieves a further 1.67% performance gain, eventually reaching an accuracy of 47.88%. This improvement trend continues in the out-of-domain evaluation scenario: in the math reasoning task, the full setting (PTS + ABS) achieves an absolute performance improvement of 2.0% compared to GRPO (48.70% vs. 46.74%, with 41.71% before post-training). In the ChartQA dataset, which has more significant distributional differences, the joint application of PTS and ABS still maintains an effective performance gain (77.04% vs. 76.20%, with 73.08% before post-training). Our method also demonstrates improved performance in HallusionBench.

Rationality of Pairwise Trajectory Sampling. One core mechanism of the PTS lies in the structured contrastive sampling scheme. To verify the effectiveness of this bidirectional optimization mechanism, we designed the following experiments: (1) one-way positive sampling (only select trajectories with highest advantage); (2) one-way negative sampling

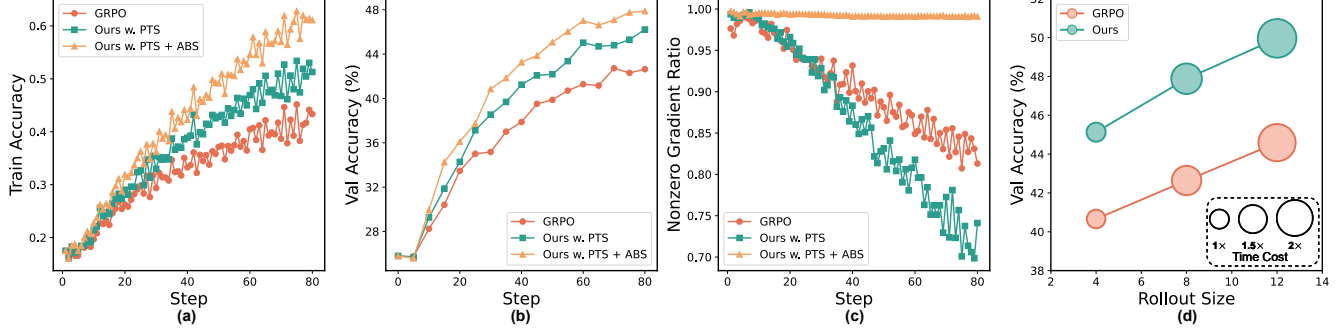


Figure 5: (a): Training accuracy of GRPO and Shuffle-R1. (b): Validation accuracy of GRPO and Shuffle-R1. (c): Token utilization rate of GRPO and Shuffle-R1. (d): Shuffle-R1 achieves better performance with minimal extra time cost.

Setting	Geo3k	Math Avg.	HallBench	ChartQA
Qwen2.5-VL-3B	25.79	41.71	59.83	73.08
+ GRPO	42.64	46.74	63.09	76.20
<i>Ablation on PTS</i>				
+ only max	41.26	44.77	63.30	75.64
+ only min	23.36	41.52	60.98	74.36
+ rand. select	43.53	46.62	63.19	76.00
+ PTS	46.21	47.64	63.40	76.52
<i>Ablation on ABS</i>				
+ rand. shuffle	46.05	47.40	63.19	76.60
+ reorder	46.28	47.64	63.09	76.64
+ ABS	47.88	48.80	63.19	77.04

Table 5: Ablation study on rationality of PTS and ABS.

(only select trajectories with lowest advantage); and (3) unbiased random sampling. All settings maintained a consistent sampling ratio (8 valid trajectories from 16 rollouts) to ensure fairness. We disable ABS since it relies on the pairing result of PTS. As shown in Tab. 5, model trained with PTS receives a consistent performance gain on both in-domain and out-of-domain tasks, while one-way positive and one-way negative sampling show a decline in all tasks, demonstrating the effectiveness and rationality of our design. Unbiased random sampling only receives minor improvement over baseline, far behind the effectiveness of PTS.

Rationality of Advantage-based Batch Shuffle. ABS introduces Advantage-aware shuffling and Inter-sub-batch resampling to reshape the training batch. To validate their effectiveness, we designed two contrastive experiments: (1) unbiased shuffle: using uniformly distributed sampling weights to perform shuffle strategy, and (2) static reorder: randomly reorder the training batch without shuffle, maintaining the original data distribution. We enable PTS during training as ABS relies on its pairing result. As shown in Tab. 5, model trained with ABS significantly outperforms the contrastive settings. The unbiased shuffle setting even performs worse compared to the PTS-only setting, demonstrating the rationality of ABS. The static reorder setting has no improvement compared to PTS-only setting, as they have the same data distribution.

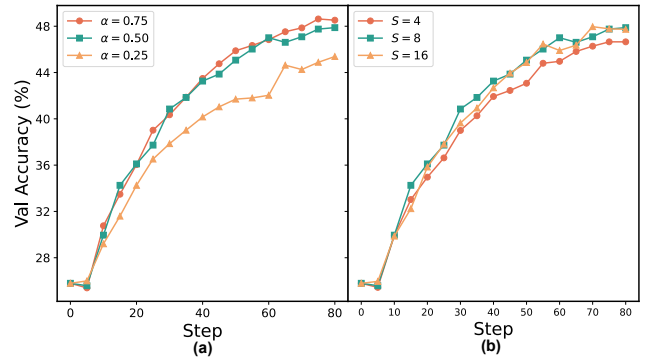


Figure 6: Ablation on key hyper parameters. (a): Effect of sampling ratio α . (b): Effect of shuffle times S .

Hyperparameters. We investigate the impact of two key hyperparameters in our framework: (1) the sampling ratio (α) in PTS, and (2) the shuffle times (S) in ABS. For α , we fix $S = 8$ and test values of 0.25, 0.5, and 0.75 (i.e., selecting 4, 8, and 12 samples from 16 rollouts). As shown in Fig. 6(a), both $\alpha = 0.75$ and $\alpha = 0.5$ yield strong performance, while $\alpha = 0.25$ lags behind. We attribute this to over-pruning, where filtering out rollouts too aggressively may reduce data diversity. We choose $\alpha = 0.5$ to strike a balance between signal quality and computational efficiency. For S , we fix $\alpha = 0.5$ and vary the shuffle times as 4, 8, and 16. Fig. 6(b) shows that performance improves with increasing S , but saturates beyond $S = 8$. This suggests that moderate resampling enhances data exposure, but too many shuffles may offer diminishing returns.

6 Conclusion

In this paper, we propose Shuffle-R1, a simple but effective framework that improves the training efficiency of reinforcement learning of multimodal large language models. Through Pairwise Trajectory Sampling and Advantage-based Batch Shuffle, our framework significantly outperforms representative algorithms and models in both in-domain and out-of-domain tasks, demonstrating the value of data-centric adaptive design. We hope that our motivations, method, and findings are helpful for further research.

References

- Achiam, J.; Adler, S.; Agarwal, S.; Ahmad, L.; Akkaya, I.; Aleman, F. L.; Almeida, D.; Altenschmidt, J.; Altman, S.; Anadkat, S.; et al. 2024. Gpt-4 technical report. arXiv:2303.08774.
- Ahmadian, A.; Cremer, C.; Gallé, M.; Fadaee, M.; Kreutzer, J.; Pietquin, O.; Üstün, A.; and Hooker, S. 2024. Back to basics: Revisiting reinforce style optimization for learning from human feedback in llms. arXiv:2402.14740.
- Allen-Zhu, Z.; and Li, Y. 2024. Physics of language models: Part 3.1, knowledge storage and extraction. arXiv:2309.14316.
- Anthropic. 2025. Claude 3.7 Sonnet, anthropic.com. <https://www.anthropic.com/clause/sonnet>. 2025-02-24.
- Bai, S.; Chen, K.; Liu, X.; Wang, J.; Ge, W.; Song, S.; Dang, K.; Wang, P.; Wang, S.; Tang, J.; et al. 2025. Qwen2. 5-vl technical report. arXiv:2502.13923.
- Chen, H.; Tu, H.; Wang, F.; Liu, H.; Tang, X.; Du, X.; Zhou, Y.; and Xie, C. 2025a. SFT or RL? An Early Investigation into Training R1-Like Reasoning Large Vision-Language Models. arXiv:2504.11468.
- Chen, Z.; Wang, W.; Cao, Y.; Liu, Y.; Gao, Z.; Cui, E.; Zhu, J.; Ye, S.; Tian, H.; Liu, Z.; et al. 2025b. Expanding performance boundaries of open-source multimodal models with model, data, and test-time scaling. arXiv:2412.05271.
- Chu, T.; Zhai, Y.; Yang, J.; Tong, S.; Xie, S.; Schuurmans, D.; Le, Q. V.; Levine, S.; and Ma, Y. 2025a. Sft memorizes, rl generalizes: A comparative study of foundation model post-training. arXiv:2501.17161.
- Chu, X.; Huang, H.; Zhang, X.; Wei, F.; and Wang, Y. 2025b. GPG: A Simple and Strong Reinforcement Learning Baseline for Model Reasoning. arXiv:2504.02546.
- Deepmind, G. 2025. Gemini 2.5: Our most intelligent AI model — blog.google. <https://blog.google/technology/google-deepmind/gemini-model-thinking-updates-march-2025/#gemini-2-5-thinking>. Accessed: 2025-03-25.
- Deng, Y.; Bansal, H.; Yin, F.; Peng, N.; Wang, W.; and Chang, K.-W. 2025. Openvlthinker: An early exploration to complex vision-language reasoning via iterative self-improvement. arXiv:2503.17352.
- Du, W.; Wang, H.; Hao, Z.; Wang, C.; Song, Y.; and Cai, Z. 2024. LLM-Augmented Deep Reinforcement Learning for Complex Task Planning. In *2024 China Automation Congress (CAC)*, 6593–6598. IEEE.
- Guan, T.; Liu, F.; Wu, X.; Xian, R.; Li, Z.; Liu, X.; Wang, X.; Chen, L.; Huang, F.; Yacoob, Y.; et al. 2024. Hallusion-bench: an advanced diagnostic suite for entangled language hallucination and visual illusion in large vision-language models. In *Proc. of IEEE Intl. Conf. on Computer Vision and Pattern Recognition*, 14375–14385.
- Guo, D.; Yang, D.; Zhang, H.; Song, J.; Zhang, R.; Xu, R.; Zhu, Q.; Ma, S.; Wang, P.; Bi, X.; et al. 2025. Deepseek-r1: Incentivizing reasoning capability in llms via reinforcement learning. arXiv:2501.12948.
- Guo, D.; Zhu, Q.; Yang, D.; Xie, Z.; Dong, K.; Zhang, W.; Chen, G.; Bi, X.; Wu, Y.; Li, Y.; et al. 2024. DeepSeek-Coder: When the Large Language Model Meets Programming-The Rise of Code Intelligence. arXiv:2401.14196.
- Hu, J. 2025. Reinforce++: A simple and efficient approach for aligning large language models. arXiv:2501.03262.
- Huang, W.; Jia, B.; Zhai, Z.; Cao, S.; Ye, Z.; Zhao, F.; Xu, Z.; Hu, Y.; and Lin, S. 2025. Vision-r1: Incentivizing reasoning capability in multimodal large language models. arXiv:2503.06749.
- Kang, K.; Setlur, A.; Ghosh, D.; Steinhardt, J.; Tomlin, C.; Levine, S.; and Kumar, A. 2024. What Do Learning Dynamics Reveal About Generalization in LLM Reasoning? arXiv:2411.07681.
- Leng, S.; Wang, J.; Li, J.; Zhang, H.; Hu, Z.; Zhang, B.; Zhang, H.; Jiang, Y.; Li, X.; Wang, F.; Rong, Y.; Sun, A.; and Lu, S. 2025. MMR1: Advancing the Frontiers of Multimodal Reasoning. <https://github.com/LengSicong/MMR1>. 2025-03-11.
- Li, X.; Yan, Z.; Meng, D.; Dong, L.; Zeng, X.; He, Y.; Wang, Y.; Qiao, Y.; Wang, Y.; and Wang, L. 2025. VideoChat-R1: Enhancing Spatio-Temporal Perception via Reinforcement Fine-Tuning. arXiv:2504.06958.
- Liu, X.; Ni, J.; Wu, Z.; Du, C.; Dou, L.; Wang, H.; Pang, T.; and Shieh, M. Q. 2025a. NoisyRollout: Reinforcing Visual Reasoning with Data Augmentation. arXiv:2504.13055.
- Liu, Y.; Peng, B.; Zhong, Z.; Yue, Z.; Lu, F.; Yu, B.; and Jia, J. 2025b. Seg-zero: Reasoning-chain guided segmentation via cognitive reinforcement. arXiv:2503.06520.
- Liu, Z.; Sun, Z.; Zang, Y.; Dong, X.; Cao, Y.; Duan, H.; Lin, D.; and Wang, J. 2025c. Visual-rft: Visual reinforcement fine-tuning. arXiv:2503.01785.
- Lu, P.; Bansal, H.; Xia, T.; Liu, J.; Li, C.; Hajishirzi, H.; Cheng, H.; Chang, K.-W.; Galley, M.; and Gao, J. 2023. MathVista: Evaluating Mathematical Reasoning of Foundation Models in Visual Contexts. In *The 3rd Workshop on Mathematical Reasoning and AI at NeurIPS'23*.
- Lu, P.; Gong, R.; Jiang, S.; Qiu, L.; Huang, S.; Liang, X.; and Zhu, S.-c. 2021. Inter-GPS: Interpretable Geometry Problem Solving with Formal Language and Symbolic Reasoning. In *Annual Meeting of the Association for Computational Linguistics*, 6774–6786.
- Ma, Y.; Du, L.; Shen, X.; Chen, S.; Li, P.; Ren, Q.; Ma, L.; Dai, Y.; Liu, P.; and Yan, J. 2025. One RL to See Them All: Visual Triple Unified Reinforcement Learning. arXiv:2505.18129.
- Masry, A.; Do, X. L.; Tan, J. Q.; Joty, S.; and Hoque, E. 2022. ChartQA: A Benchmark for Question Answering about Charts with Visual and Logical Reasoning. In *Annual Meeting of the Association for Computational Linguistics*, 2263–2279.
- Meng, F.; Du, L.; Liu, Z.; Zhou, Z.; Lu, Q.; Fu, D.; Han, T.; Shi, B.; Wang, W.; He, J.; et al. 2025. MM-Eureka: Exploring the Frontiers of Multimodal Reasoning with Rule-based Reinforcement Learning. arXiv:2503.07365.

- Muennighoff, N.; Yang, Z.; Shi, W.; Li, X. L.; Fei-Fei, L.; Hajishirzi, H.; Zettlemoyer, L.; Liang, P.; Candès, E.; and Hashimoto, T. 2025. s1: Simple test-time scaling. *arXiv preprint arXiv:2501.19393*.
- OpenAI. 2024. OpenAI o1 System Card — openai.com. <https://cdn.openai.com/o1-system-card.pdf>. Accessed: 2024-09-12.
- Peng, Y.; Zhang, G.; Zhang, M.; You, Z.; Liu, J.; Zhu, Q.; Yang, K.; Xu, X.; Geng, X.; and Yang, X. 2025. LMM-R1: Empowering 3B LMMs with Strong Reasoning Abilities Through Two-Stage Rule-Based RL. *arXiv:2503.07536*.
- Qiao, R.; Tan, Q.; Dong, G.; Wu, M.; Sun, C.; Song, X.; GongQue, Z.; Lei, S.; Wei, Z.; Zhang, M.; et al. 2024. We-math: Does your large multimodal model achieve human-like mathematical reasoning? *arXiv:2407.01284*.
- Seed, B.; Yuan, Y.; Yue, Y.; Wang, M.; Zuo, X.; Chen, J.; Yan, L.; Xu, W.; Zhang, C.; Liu, X.; et al. 2025. Seed-thinking-v1.5: Advancing superb reasoning models with reinforcement learning. *arXiv:2504.13914*.
- Shao, Z.; Wang, P.; Zhu, Q.; Xu, R.; Song, J.; Bi, X.; Zhang, H.; Zhang, M.; Li, Y.; Wu, Y.; et al. 2024. Deepseekmath: Pushing the limits of mathematical reasoning in open language models. *arXiv:2402.03300*.
- Tan, H.; Ji, Y.; Hao, X.; Lin, M.; Wang, P.; Wang, Z.; and Zhang, S. 2025. Reason-rft: Reinforcement fine-tuning for visual reasoning. *arXiv:2503.20752*.
- Team, K.; Du, A.; Gao, B.; Xing, B.; Jiang, C.; Chen, C.; Li, C.; Xiao, C.; Du, C.; Liao, C.; et al. 2025. Kimi k1.5: Scaling reinforcement learning with llms. *arXiv:2501.12599*.
- Thawakar, O.; Dissanayake, D.; More, K.; Thawkar, R.; Heakl, A.; Ahsan, N.; Li, Y.; Zumri, M.; Lahoud, J.; Anwer, R. M.; et al. 2025. Llamav-o1: Rethinking step-by-step visual reasoning in llms. *arXiv:2501.06186*.
- Wang, H.; Qu, C.; Huang, Z.; Chu, W.; Lin, F.; and Chen, W. 2025a. VL-Rethinker: Incentivizing Self-Reflection of Vision-Language Models with Reinforcement Learning. *arXiv:2504.08837*.
- Wang, K.; Pan, J.; Shi, W.; Lu, Z.; Ren, H.; Zhou, A.; Zhan, M.; and Li, H. 2024. Measuring multimodal mathematical reasoning with math-vision dataset. In *Proc. of Advances in Neural Information Processing Systems*, volume 37, 95095–95169.
- Wang, X.; Yang, Z.; Feng, C.; Lu, H.; Li, L.; Lin, C.-C.; Lin, K.; Huang, F.; and Wang, L. 2025b. SoTA with Less: MCTS-Guided Sample Selection for Data-Efficient Visual Reasoning Self-Improvement. *arXiv:2504.07934*.
- Wang, Y.; Xu, B.; Yue, Z.; Xiao, Z.; Wang, Z.; Zhang, L.; Yang, D.; Wang, W.; and Jin, Q. 2025c. Time-R1: Post-Training Large Vision Language Model for Temporal Video Grounding. *arXiv:2503.13377*.
- Wu, Q.; Yang, X.; Zhou, Y.; Fang, C.; Song, B.; Sun, X.; and Ji, R. 2025. Grounded Chain-of-Thought for Multimodal Large Language Models. *arXiv:2503.12799*.
- Xu, G.; Jin, P.; Hao, L.; Song, Y.; Sun, L.; and Yuan, L. 2025. Llava-o1: Let vision language models reason step-by-step. *arXiv:2411.10440*.
- Yang, Y.; He, X.; Pan, H.; Jiang, X.; Deng, Y.; Yang, X.; Lu, H.; Yin, D.; Rao, F.; Zhu, M.; et al. 2025. R1-onevision: Advancing generalized multimodal reasoning through cross-modal formalization. *arXiv:2503.10615*.
- Yao, H.; Huang, J.; Wu, W.; Zhang, J.; Wang, Y.; Liu, S.; Wang, Y.; Song, Y.; Feng, H.; Shen, L.; et al. 2024. Mulberry: Empowering mllm with o1-like reasoning and reflection via collective monte carlo tree search. *arXiv:2412.18319*.
- Yao, H.; Yin, Q.; Zhang, J.; Yang, M.; Wang, Y.; Wu, W.; Su, F.; Shen, L.; Qiu, M.; Tao, D.; et al. 2025. R1-ShareVL: Incentivizing Reasoning Capability of Multimodal Large Language Models via Share-GRPO. *arXiv:2505.16673*.
- Yao, S.; Yu, D.; Zhao, J.; Shafran, I.; Griffiths, T.; Cao, Y.; and Narasimhan, K. 2023. Tree of thoughts: Deliberate problem solving with large language models. In *Proc. of Advances in Neural Information Processing Systems*, volume 36, 11809–11822.
- Yaowei, Z.; Junting, L.; Shenzhi, W.; Zhangchi, F.; Dong-dong, K.; and Yuwen, X. 2025. EasyR1: An Efficient, Scalable, Multi-Modality RL Training Framework. <https://github.com/hiyouga/EasyR1>.
- Ye, T.; Xu, Z.; Li, Y.; and Allen-Zhu, Z. 2024. Physics of language models: Part 2.1, grade-school math and the hidden reasoning process. In *Proc. of Intl. Conf. on Learning Representations*.
- Ye, Y.; Huang, Z.; Xiao, Y.; Chern, E.; Xia, S.; and Liu, P. 2025. LIMO: Less is More for Reasoning. *arXiv:2501.19393*.
- Yu, Q.; Zhang, Z.; Zhu, R.; Yuan, Y.; Zuo, X.; Yue, Y.; Fan, T.; Liu, G.; Liu, L.; Liu, X.; et al. 2025. DAPO: An open-source llm reinforcement learning system at scale. *arXiv:2503.14476*.
- Yue, X.; Qu, X.; Zhang, G.; Fu, Y.; Huang, W.; Sun, H.; Su, Y.; and Chen, W. 2024. MAMmoTH: Building Math Generalist Models through Hybrid Instruction Tuning. In *Proc. of Intl. Conf. on Learning Representations*.
- Zhang, D.; Zhoubian, S.; Hu, Z.; Yue, Y.; Dong, Y.; and Tang, J. 2024a. Rest-mcts*: Llm self-training via process reward guided tree search. In *Proc. of Advances in Neural Information Processing Systems*, volume 37, 64735–64772.
- Zhang, J.; Huang, J.; Yao, H.; Liu, S.; Zhang, X.; Lu, S.; and Tao, D. 2025. R1-vl: Learning to reason with multimodal large language models via step-wise group relative policy optimization. *arXiv:2503.12937*.
- Zhang, R.; Jiang, D.; Zhang, Y.; Lin, H.; Guo, Z.; Qiu, P.; Zhou, A.; Lu, P.; Chang, K.-W.; Qiao, Y.; et al. 2024b. Mathverse: Does your multi-modal llm truly see the diagrams in visual math problems? In *Proc. of European Conference on Computer Vision*, 169–186. Springer.
- Zhu, J.; Wang, W.; Chen, Z.; Liu, Z.; Ye, S.; Gu, L.; Duan, Y.; Tian, H.; Su, W.; Shao, J.; et al. 2025. InternVL3: Exploring Advanced Training and Test-Time Recipes for Open-Source Multimodal Models. *arXiv:2504.10479*.

A Pseudo Code

Here, we provide the pseudo code of Shuffle-R1 for readers to better understand the pipeline flow, and for better transparency in algorithm understanding and reproducibility.

Algorithm 1: Shuffle-R1 Workflow

```

1: Input:  $\mathcal{Q}$  (queries),  $\pi_\theta$  (policy),  $2N$  (rollouts per query),  $\alpha$  (sampling ratio),  $S$  (shuffle rounds)
2: Output: Optimized batch  $\mathcal{B}'$  for gradient update
3: Initialize global batch  $\mathcal{B} \leftarrow \emptyset$ 
4: for each  $q \in \mathcal{Q}$  do ▷ PTS Phase
5:   Generate  $\{o_i\}_{i=1}^{2N} \sim \pi_\theta(q)$ 
6:   Compute  $\{\hat{A}_i\}$  via  $R = RewardFunc(\{o_i\}, q)$ 
7:   Sort pairs:  $\{(o_{(i)}, o_{(2N-i+1)})\}_{i=1}^N \leftarrow \text{MaxMinPair}(\{\hat{A}_i\})$ 
8:   Retain top- $\lfloor \alpha N \rfloor$  pairs:  $\mathcal{B}_q \leftarrow \{(o_{(k)}, o_{(2N-k+1)})\}_{k=1}^{\lfloor \alpha N \rfloor}$ 
9:   Aggregate:  $\mathcal{B} \leftarrow \mathcal{B} \cup \mathcal{B}_q$ 
10: end for
11: Compute  $W_j = |\hat{A}_p| + |\hat{A}_q| \forall (o_p, o_q) \in \mathcal{B}$  ▷ ABS Phase
12: Calculate  $P_j = W_j / \sum W_k$  for weighted sampling
13:  $\mathcal{B}' \leftarrow \text{ShuffleSample}(\mathcal{B}, P_j, S)$  with  $S \times T = |\mathcal{B}|$ 
14: return  $\mathcal{B}'$  ▷ Jointly optimized training data
```

B Prompt Design

We use a “Thinking prompt” to explicitly control the output format of the model, which requires the model to output its thinking process within special tokens `<think>` and `</think>`, and mark the final answer with `\boxed{}`. In practice, we keep the system prompt of Qwen2.5-VL (Bai et al. 2025), and insert the “Thinking prompt” at the beginning of user message. We keep the training and evaluation prompt in the same format. The full structure of instruction prompt is as follows:

Prompt Example

SYSTEM:
You are a helpful assistant.

USER:
You FIRST think about the reasoning process as an internal monologue and then provide the final answer. The reasoning process MUST BE enclosed within `<think>` `</think>` tags. The final answer MUST BE put in `\boxed{}`. <QUESTION>

C Experiment Settings

We report details of our training and evaluation settings here, including reward function design, main hyperparameters and computing resources.

Reward Calculation. We adopt a combination of format reward and accuracy reward as the final reward in reinforcement learning. The format reward and accuracy reward are calculated as follows:

$$r_{\text{format}} = \begin{cases} 1, & \text{if format is } \textit{correct} \\ 0, & \text{if format is } \textit{incorrect} \end{cases} \quad (11)$$

Hyperparameters	Value
max pixels	1000000
min pixels	262144
max prompt length	2048
max response length	2048
rollout batch size	512
global batch size	128
learning rate	1e-6
optimizer	AdamW
rollout temperature	1.0
rollout top p	0.99
evaluation temperature	0.5
rollout group number	16
PTS sampling ratio (α)	0.5
ABS shuffle times (S)	8
KL coefficient	0.0
vision encoder	frozen

Table 6: Hyperparameter settings.

$$r_{\text{acc}} = \begin{cases} 1, & \text{if answer = ground truth} \\ 0, & \text{if answer } \neq \text{ ground truth} \end{cases} \quad (12)$$

The final reward is the weighted sum of above rewards:

$$r_{\text{overall}} = 0.1 \times r_{\text{format}} + 0.9 \times r_{\text{acc}} \quad (13)$$

Format reward is assigned to a smaller weight since response formatting is easy to learn.

Hyperparameters. We use EasyR1 (Yaowei et al. 2025) as our training framework. Full hyperparameter settings during training is shown in Tab. 6. For experiments on Geometry3K and K12 with $\sim 2.1k$ training samples, we set the training steps to 80. For the joint training experiments ($\sim 30k$ training samples), we increase the training steps to 150 due to extended data size. Other hyperparameters that are not mentioned are kept to default values of EasyR1.

Computing Resources. All experiments are conducted on $8 \times$ NVIDIA H800-80G-SXM GPUs.

D Dataset Collection

For training dataset, we choose Geometry3K (Lu et al. 2021) and MMK12 dataset. Geometry3K dataset is a high quality real-world geometry problem solving dataset, containing 2.1K training samples and 601 test samples. It contains a wide range of geometry problems with varying levels of difficulty. The text problems are very compact with most of the geometric conditions represented in images, making it suitable for our training. MMK12 dataset is introduced by MM-Eureka (Meng et al. 2025), which contains 16k math reasoning training samples. The training samples have both geometric and non-geometric problems and have been carefully examined and manually filtered to ensure quality. The test set of MMK12 further includes other STEM problems such as physics, biology and chemistry. During our training, we used a randomly selected subset of MMK12 provided by NoisyRollout (Liu et al. 2025a) (referred to as ‘K12’ in the paper to distinguish it from full set of MMK12), which

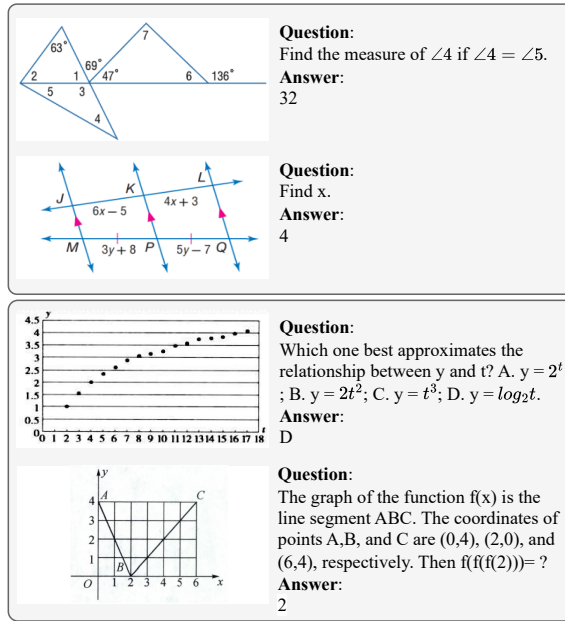


Figure 7: Top: Examples of Geometry3K. Bottom: Examples of MMK12.

has 2.1k samples with the same size as Geometry3K. All the training samples are in free-form format. Examples of training data shown in Fig. 7.

To fully evaluate model’s reasoning ability, apart from in-domain test set from training dataset, we select several representative benchmarks to examine model’s performance on math reasoning, visual perception, and chart understanding tasks. For math reasoning task, we choose MathVerse (Zhang et al. 2024b), MathVision (Wang et al. 2024), WeMath (Qiao et al. 2024) and MathVista (Lu et al. 2023). We choose HallusionBench (Guan et al. 2024) and ChartQA (Masry et al. 2022) for visual perception and chart understanding tasks respectively. We believe that a good RL algorithm can not only improve in-domain performance, but also have the potential to promote robust generalization to out-of-domain tasks. Examples of evaluation data shown in Fig. 8.

E Evaluation Metrics

We adopt pass@1 accuracy as evaluation metric. During evaluation, we set the decoding temperature to 0.5 and perform 8 independent runs, reporting the average pass@1 accuracy as final metric. The choice of temperature doesn’t degrade model performance, and the averaged accuracy reduces the randomness, resulting in a more stable and reliable evaluation. Prompt format for evaluation is kept identical to training prompt. Evaluation settings of our model and all the reproduced results in main paper are kept the same to ensure a fair comparison.

For evaluation of MathVerse, MathVision, WeMath, MathVista and ChartQA, we employ Gemini-2.0-Flash-001 (Deepmind 2025) to first extract the predicted answer

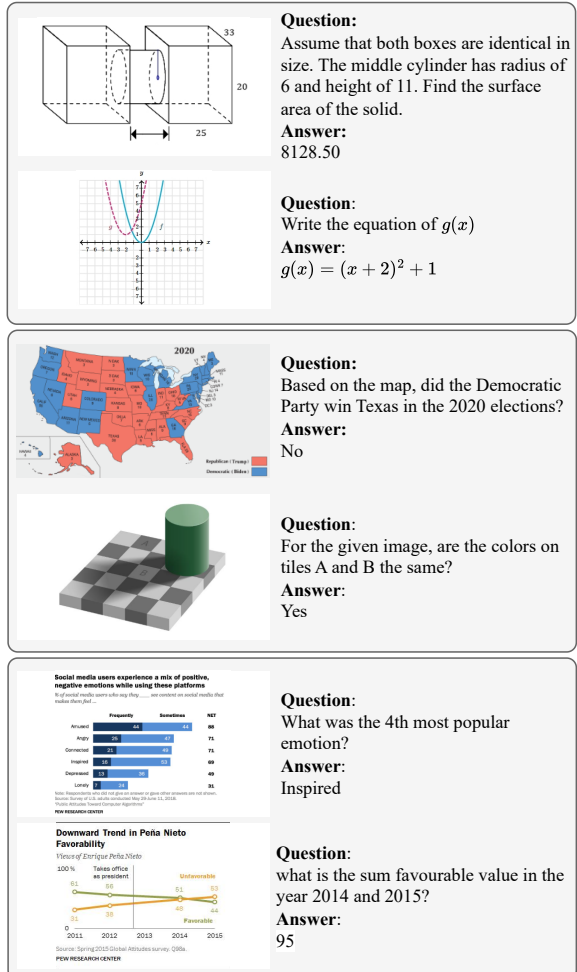


Figure 8: Top: Examples of math reasoning tasks. Middle: Examples of visual perception tasks. Bottom: Examples of chart understanding tasks.

from model response then compare it with ground truth. Fig. 9 and Fig. 10 demonstrate the extraction and verification prompt for Gemini. Specifically, we report accuracy on WeMath under loose mode, and overall accuracy on MathVerse (including all sub categories: Text Dominant, Text Lite, Vision Intensive, Vision Dominant and Vision Only).

F More Experimental Results

Detailed Model Performance. We provide a more detailed performance of models trained on Geometry3K and K12 dataset in Tab. 7, reporting model performance on each out-of-domain benchmarks as a supplement to “Math Avg.” columns in main paper. Trained with only 2.1k data, both the 3B and 7B model demonstrate significant performance gains.

Comparison with more RL algorithms. We provide additional comparisons with more representative RL algorithms, i.e. RLOO (Ahmadian et al. 2024) and REINFORCE++ (Hu 2025). We conduct experiments on

Please read the following example.
Then output the answer extracted from the model response directly. No "Extracted answer:" in your answer.

Hint: Please answer the question requiring an integer answer and provide the final value, e.g., 1, 2, 3, at the end.
Question: Which number is missing?
Model response: The number missing in the sequence is 14.
Extracted answer: 14

Hint: Please answer the question requiring a floating-point number with one decimal place and provide the final value, e.g., 1.2, 1.3, 1.4, at the end.
Question: What is the fraction of females facing the camera?
Model response: The fraction of females facing the camera is 0.6, which means that six out of ten females in the group are facing the camera.
Extracted answer: 0.6

Hint: Please answer the question requiring a floating-point number with two decimal places and provide the final value, e.g., 1.23, 1.34, 1.45, at the end.
Question: How much money does Luca need to buy a sour apple candy and a butter-scotch candy? (Unit: \$)
Model response: Luca needs \$1.45 to buy a sour apple candy and a butterscotch candy.
Extracted answer: 1.45

Hint: Please answer the question requiring a Python list as an answer and provide the final list, e.g., [1, 2, 3], [1.2, 1.3, 1.4], at the end.
Question: Between which two years does the line graph saw its maximum peak?
Model response: The line graph saw its maximum peak between 2007 and 2008.
Extracted answer: [2007, 2008]

Hint: Please answer the question and provide the correct option letter, e.g., A, B, C, D, at the end.
Question: What fraction of the shape is blue?
Choices: (A) 3/11 (B) 8/11 (C) 6/11 (D) 3/5
Model response: The correct answer is (B) 8/11.
Extracted answer: B

QUESTION
Model response: **PREDICTION**
Extracted answer:

Figure 9: Extraction prompt for Gemini.

Below are two answers to a math question/chart understanding question. Question is [Question], [Standard Answer] is the standard answer to the question, and [Model_answer] is the answer extracted from a model's output to this question. Determine whether these two answers are consistent. Please note that only when the [Model_answer] completely matches the [Standard Answer] means they are consistent. For non-multiple-choice questions, if the meaning is expressed in the same way, it is also considered consistent, for example, 0.5m and 50cm.
If they are consistent, Judgement is 1; if they are different, Judgement is 0.

[Question]: Write the set of numbers represented on the number line in interval notation.
[Standard Answer]: (-2, 1]
[Model_answer]: Extracted Answer: '((-2, 1))
Judgement: 0

[Question]: As shown in the figure, circle O has a radius 1.0, if angle BAC = 60.0, then the length of BC is ()
Choices:
A:2 B:2\sqrt{3} C:\sqrt{3} D:2\sqrt{2}
[Standard Answer]: C
[Model_answer]: B:2\sqrt{3}
Judgement: 0

[Question]: Find the domain and range of the function f using interval notation.
[Standard Answer]: domain: [-4, 0) and range: (-3, 1]
[Model_answer]: Range: '((-4, 1])
Judgement: 0

[Question]: As shown in the figure, circle O has a radius 1.0, if angle BAC = 60.0, then the length of BC is ()
Choices:
(A):2 (B):2\sqrt{3} (C):\sqrt{3} (D):2\sqrt{2}
[Standard Answer]: (C)
[Model_answer]: C
Judgement: 1

Please output the judgement score directly with no explanation.
[Question]: **QUESTION**
[Standard Answer]: **ANSWER**
[Model_answer]: **PREDICTION**
Judgement:

Figure 10: Score prompt for Gemini.

Qwen2.5-VL-3B-Instruct with Geometry3K dataset. All the experiment settings are kept the same as GRPO and DAPO in main paper. The final model performance is shown in Tab. 8. Our framework outperform these algorithms by a large margin in both in-domain and out-of-domain tasks.

Comparison with Direct Experience Replay. We conduct a comparative study by replacing ABS with a prioritized experience replay mechanism. Experience replay maintains a decoupled buffer of past samples, whereas ABS adopts an online, in-place shuffle strategy to dynamically reshape the data distribution. As shown in Fig. 11(a) and (b), in the later stages, the experience replay setting exhibits a plateau in training accuracy and even a drop in validation accuracy, indicating potential overfitting to stale samples. This suggests that prioritized experience replay may overly emphasize historical trajectories, leading to suboptimal convergence. Moreover, ABS proves to be more effective in mitigating the Rollout Silencing.

G Case Study

Here we provide some qualitative case study of Shuffle-R1's reasoning outputs.

Fig. 12 and Fig. 13 show two improved cases on math related tasks. In case 1, the base model has an error in visual information parsing, referring to angles not existed in the figure, resulting in a reasoning fault. The RL model correctly parsed and solved the geometry problem. In case 2, the base model misused a geometric theorem, leading to wrong answer, while the RL model correctly solved the problem with accurate theorem.

Fig. 14 demonstrates improved reasoning ability in RL model, where the base model has accurate perception about the chart but has reasoning error in CoT. The RL model can not only accurately parse the visual information, but also perform correct reasoning to finally reach the right answer.

Case 4 in Fig. 15 further demonstrates that RL model also has better visual perception ability compared to base model. The figure from HallusionBench has been artificially inserted with an image of a hen, which only occupies a very small region of the original image. This modification has resulted in a perception error and in base model, but the RL model can accurately identify the inserted image.

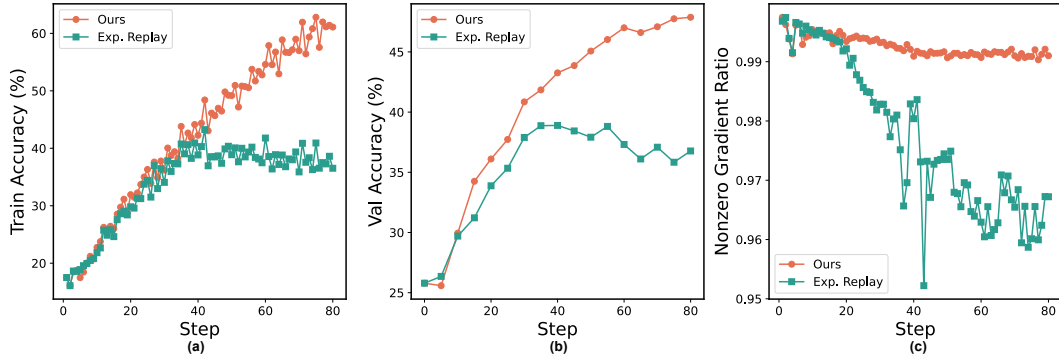


Figure 11: Performance of Shuffle-R1 compared with directly applying Prioritized Experience Replay.

Method	MathVerse	MathVision	MathVista	WeMath	HallBench	ChartQA	Total Avg.
Qwen2.5-VL-3B	34.77	21.94	58.40	51.72	59.83	73.08	49.96
+ Ours (Geo3K)	43.55	25.30	61.80	64.14	63.19	77.04	55.84
+ Ours (K12)	44.06	26.48	64.90	64.77	65.72	78.28	57.37
Qwen2.5-VL-7B	42.59	25.76	67.40	63.51	65.19	79.84	57.38
+ Ours (Geo3K)	50.96	27.47	70.90	69.19	69.51	81.64	61.61
+ Ours (K12)	48.59	28.61	73.20	69.71	69.87	82.60	62.09

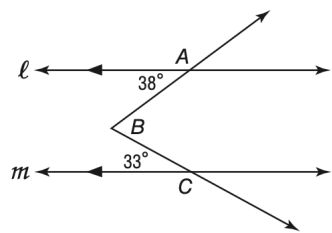
Table 7: Detailed performance on out-of-domain benchmarks of models trained on Geometry3K and K12 data. Highest accuracy marked in **Bold**.

Method	Geo3K	MathVerse	MathVision	MathVista	WeMath	HallBench	ChartQA
Qwen2.5-VL-3B	25.79	34.77	21.94	58.40	51.72	59.83	73.08
+ RLOO	42.09	39.94	22.96	58.90	59.48	64.24	76.68
+ REINFORCE++	41.76	41.70	24.86	60.90	63.51	62.99	76.20
+ Ours	47.88	43.55	25.30	61.80	64.14	63.19	77.04

Table 8: Performance of Shuffle-R1 on Geometry3K dataset compared with RLOO and REINFORCE++. Highest accuracy marked in **Bold**.

 **USER Input**

In the figure below, $\angle ABC$ is intersected by parallel lines l and m . What is the measure of $\angle ABC$? Express your answer in degrees.



 **Base Model** 

<think>To solve for the measure of $\angle ABC$, we need to use the properties of angles formed by a transversal intersecting parallel lines. 1. Identify the given information: $\angle BAC = 38^\circ$; $\angle ACB = 33^\circ$; The lines l and m are parallel. 2. Recall that the sum of the angles in a triangle is always 180° . 3. Therefore, we can write the equation for the sum of the angles in triangle ABC :

$$\angle BAC + \angle ABC + \angle ACB = 180^\circ$$
 4. Substitute the given values into the equation:

$$38^\circ + \angle ABC + 33^\circ = 180^\circ$$
 5. Simplify the equation:

$$71^\circ + \angle ABC = 180^\circ$$
 6. Solve for $\angle ABC$:

$$\angle ABC = 180^\circ - 71^\circ = 109^\circ$$
 Thus, the measure of $\angle ABC$ is **109**.

 **RL Model** 

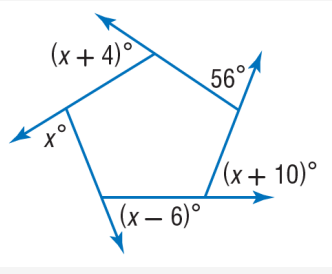
<think>Since lines l and m are parallel, $\angle ABC$ can be found by considering the angles formed by the intersection of the transversal BC with the parallel lines l and m . Specifically, $\angle ABC$ is the included angle between the two lines, and it can be calculated by adding the adjacent angles on either side of the vertex B . Here, $\angle ABC$ is the included angle between the two lines, and it can be calculated by adding the adjacent angles on either side of the vertex B . Since $\angle ABC$ is the included angle between the two lines, and it can be calculated by adding the adjacent angles on either side of the vertex B . Thus, the measure of $\angle ABC$ is the sum of the two given angles: $\angle ABC = 38^\circ + 33^\circ = 71^\circ$.</think>

71

Figure 12: A case study on math related task.

 **USER Input**

Find the value of x



 **Base Model** 

To find the value of x , we need to use the fact that the sum of the interior angles of a pentagon is 540° . The pentagon is divided into three triangles, and we can use the fact that the sum of the angles in each triangle is 180° . First, let's label the angles in the pentagon: One angle is x° . Another angle is $(x+4)^\circ$. Another angle is 56° . Another angle is $(x+10)^\circ$. The remaining angle is $(x-6)^\circ$. The sum of the interior angles of the pentagon is:

$$x + (x+4) + 56 + (x+10) + (x-6) = 540$$
 . Simplify the left side:

$$x + x + 4 + 56 + x + 10 + x - 6 = 540$$
, i.e.

$$4x + 64 = 540$$
. Subtract 64 from both sides:

$$4x = 476$$
. Divide by 4:

$$x = 119$$
. So, the value of x is **119**.

 **RL Model** 

<think>The sum of the interior angles of a quadrilateral is 360 degrees. We can set up an equation using the given expressions for the angles:

$$x + (x+4) + 56 + (x+10) + (x-6) = 360$$
 . Simplifying the left side:

$$x + x + 4 + 56 + x + 10 + x - 6 = 360$$
, i.e.

$$4x + 64 = 360$$
. Subtracting 64 from both sides:

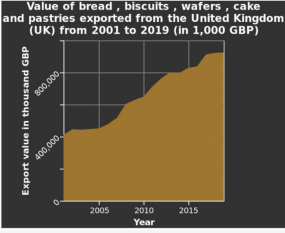
$$4x = 296$$
. Dividing both sides by 4:

$$x = 74$$
. Thus, the value of x is **74**.</think>

Figure 13: Another case study on math related task.

 **USER Input**

From 2001 to 2010, Is 2005 exported the most value of bread, biscuits, wafers, cakes and pastries from the UK? You final answer can only be yes or no.



Year	Export value in thousands GBP
2001	~400,000
2005	~450,000
2010	~500,000
2015	~550,000
2019	~600,000

 **Base Model**

<think>To determine if 2005 had the highest export value of bread, biscuits, wafers, cakes, and pastries from the UK from 2001 to 2010, we need to analyze the trend of the export value over this period. From the graph: The export value starts at around 400,000 GBP in 2001; It increases steadily until 2005. After 2005, the export value continues to increase but at a slower rate compared to the period before 2005. Since the export value is continuously increasing from 2001 to 2005 and then continues to increase but at a slower rate, it is reasonable to conclude that the highest value was reached in 2005. Final answer: yes.</think> **Yes**

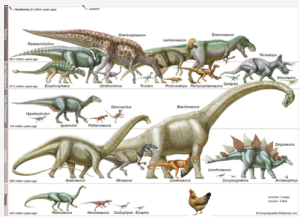
 **RL Model**

<think>From the graph, the export value in 2005 appears to be higher than in 2001 but lower than in 2010. The graph shows a general upward trend, and while 2005 is higher than 2001, it is not the peak value between 2001 and 2010. The peak value in this interval seems to be around 2010.</think> **No**

Figure 14: A case study on chart understanding task.

 **USER Input**

Are there any hens in this figure? You final answer can only be yes or no.



 **Base Model**

<think>The image is a diagram of various dinosaurs, including both herbivores and carnivores, as well as a small bird-like creature. The bird-like creature is labeled as "Archaeopteryx" which is a transitional fossil between dinosaurs and birds. There are no hens depicted in the image. Hens are domesticated chickens, which are not shown in this diagram.</think> **No**

 **RL Model**

<think>The image is a diagram of various dinosaurs and their evolutionary relationships. It includes a timeline showing the timeline of dinosaur evolution and a visual representation of different dinosaur species. There is also a chicken depicted at the bottom right corner of the image, which is not a dinosaur but a modern bird.</think> **Yes**

Figure 15: A case study on visual perception task.